THE ASTROPHYSICAL JOURNAL, 466:529–536, 1996 July 20

OBSERVATION AND MODELING OF SOFT X-RAY BRIGHT POINTS. I. INITIAL RESULTS

CHARLES C. KANKELBORG AND ARTHUR B. C. WALKER II
Department of Physics and Applied Physics, Stanford University, Stanford, CA 94305-4060
RICHARD B. HOOVER
NASA/Marshall Space Flight Center, Huntsville, AL 35812
AND
TROY W. BARBEE, JR.
Lawrence Livermore National Laboratory, Livermore, CA 94550
Received 1995 July 17; accepted 1996 February 7

ABSTRACT

The Multi-Spectral Solar Telescope Array was launched from White Sands Missile Range, New Mexico, on 1991 May 13 at 1905 UT. Full-disk, high-resoluton solar images were obtained in a variety of soft X-ray and far-ultraviolet wavelengths. The 193 Å (Fe XII) and 44 Å (Si XII) images show a large number of coronal bright points. The high spatial resolution of the Fe XII image allows many of the bright points to be resolved as tiny loops. Co-alignment of the soft X-ray images with the 1216 Å Lyα image reveals that all the coronal bright points have counterparts in the transition region, often resolved as a pair of footpoints, which are brighter than neighboring elements of the chromospheric network. Moreover, comparison with the KPNO magnetogram shows dipole structures coincident with nearly all of the bright points. We present a quantitative analysis based on preliminary photometry of four of the bright points that were observed. By fitting a simple, numerical loop model to the photometric data, we estimate the magnitude of the coronal heating in these structures. The rate of heating per unit footpoint area is found to be similar to previous measurements for much larger coronal structures. Implications for heating of the chromosphere and lower transition region are also discussed.

Subject headings: Sun: corona — Sun: magnetic fields — Sun: transition region — Sun: X-rays, gamma rays

1. INTRODUCTION

X-ray bright points (XBPs) are compact ($< 1'$), closed-field coronal structures with intense soft X-ray emission (Golub 1980). They occur both in quiet-Sun regions and in coronal holes (Habbal, Dowdy, & Withbroe 1990). Most XBPs have lifetimes on the order of a few hours, during which they exhibit chaotic variability in brightness, on timescales as short as a few minutes, with occasional flaring events (Habbal & Withbroe 1981; Habbal et al. 1990; Strong et al. 1992).

The development of ultra–high-resolution soft X-ray telescopes that use normal-incidence, multilayer mirrors (Walker et al. 1988, 1990; Golub et al. 1990) has made it possible to observe the morphology of fine-scale structures at unprecedented resolution. The Multi-Spectral Solar Telescope Array (MSSTA), a rocket-borne array of multilayer XUV and far-ultraviolet (FUV) telescopes (see Walker et al. 1990), flew at 1900 UT on 1991 May 13, obtaining photographically recorded images of the Sun at a variety of coronal and transition-region wavelengths (Walker et al. 1993). Preliminary photometric calibrations of the photograpic films used in the MSSTA rocket payload (see Hoover et al. 1991) have permitted a quantitative treatment of the heating of coronal structures observed during the 1991 May flight.

This paper is concerned with XBPs as they relate to the heating of the corona and transition region. We hope that a knowledge of the energetics of the smallest observed coronal structures will place useful constraints on the coronal heating mechanism and provide a means of probing the energy balance in the transition region and chromosphere.

2. OBSERVATIONS

The MSSTA 193 Å (Fe XII) and 1216 Å hydrogen Lyα images have been co-registered to within $\sim 3''$ using the limb and a limb prominence (bright in Lyα but dark in Fe XII) as reference points. The KPNO magnetogram was rotated to correspond with 1905 UT by K. Harvey of Solar Physics Research Corporation. The MSSTA images were then co-aligned with the magnetogram to within $\sim 10''$, using the limb and several other reference features.

Four XBPs were analyzed in detail. Figure 1 (Plate 15) is the 193 Å image obtained by the MSSTA payload, with arrows indicating the positions of the four bright points. Figure 2 (Plate 16) is the 1216 Å image. Figures 3–5 show the bright points in 193 Å (Fe XII), 1216 Å (H Lyα), and the Kitt Peak magnetogram, respectively. The XBPs (except "A") appear elongated in the Fe XII image, and some are clearly arc-shaped. The Lyα images show two bright footpoints for points B and C; the other two XBPs appear as elongated brightenings in Lyα, probably indicating the presence of two unresolved footpoints.

Bright points are normally associated with magnetic dipoles (Moses et al. 1994). The magnetogram shows a strong magnetic dipole beneath each of the XBPs. There are two magnetic dipoles near point C, but one is much closer to the observed Fe XII feature. Thus, the observational data identify these bright points as tiny coronal loops. It is noteworthy that the magnetic axes of some of the XBPs

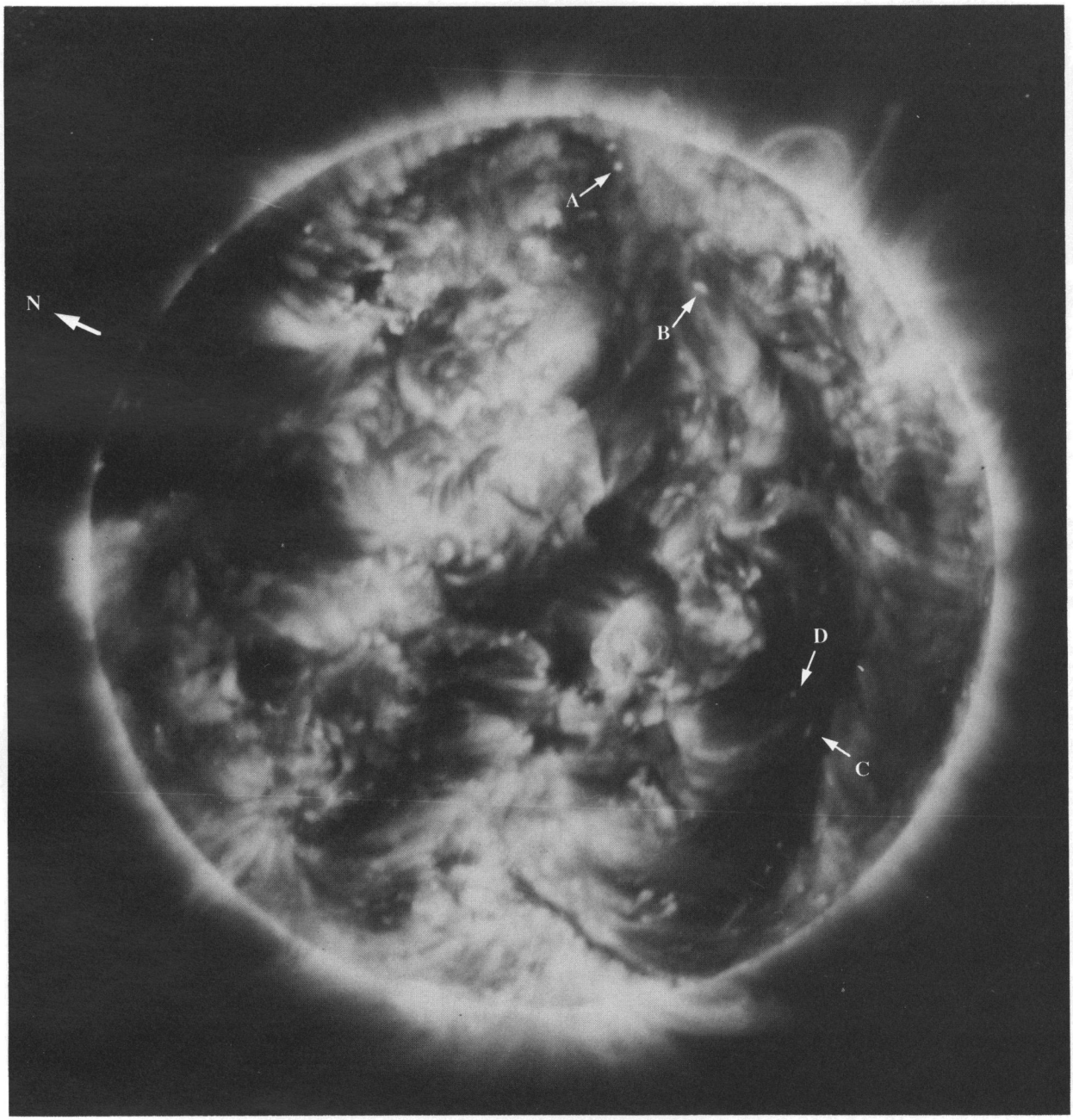

FIG. 1.—Image taken by the 193 Å (Fe XII) large Herschellian telescope, 120 s exposure. Four bright points, labeled A, B, C, and D, are examined in this paper.

PLATE 16

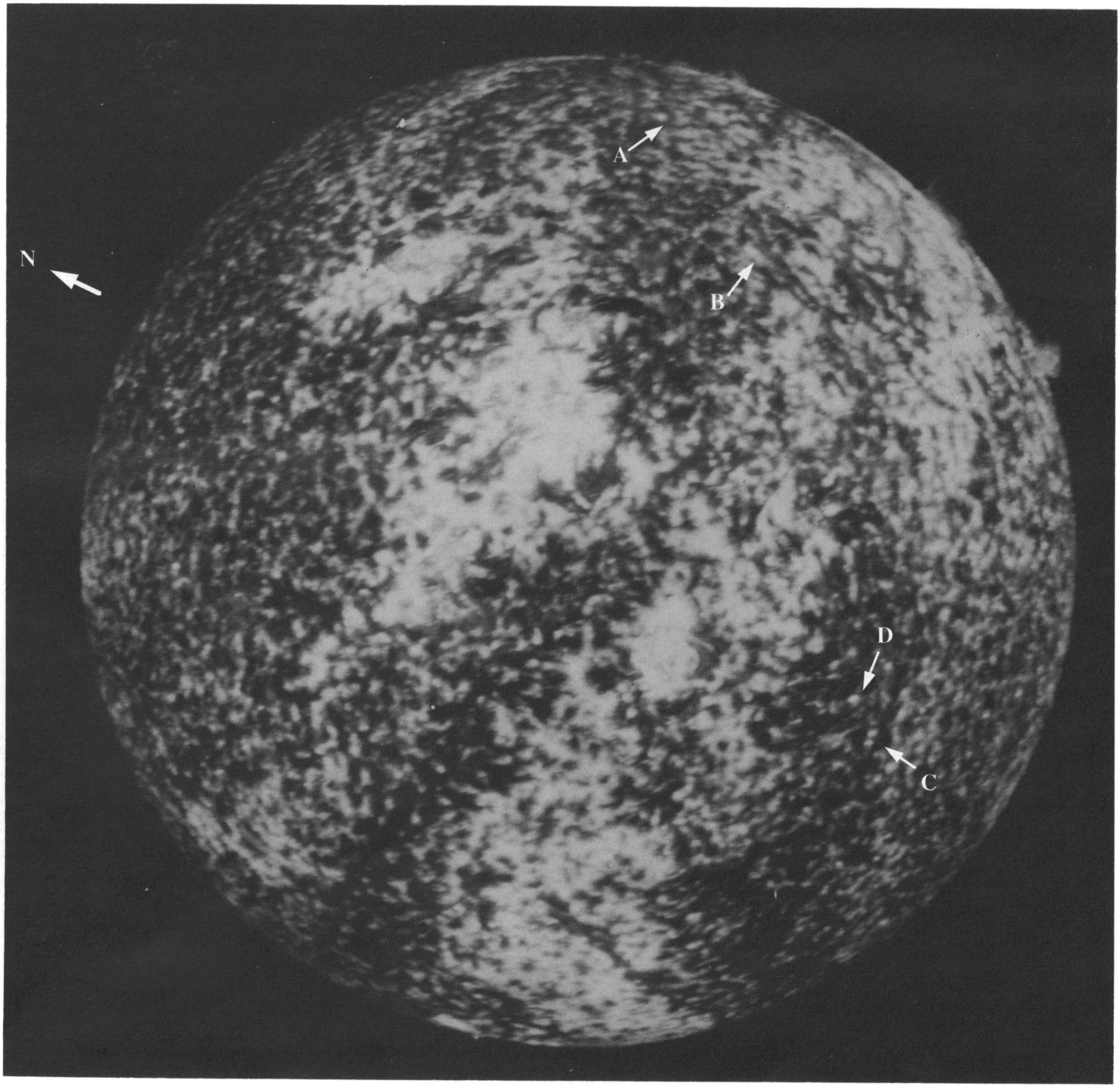

FIG. 2.—Image taken by the 1216 Å (H Lyα) Ritchey-Chrétien telescope, 120 s exposure. The footpoints of the four XBPs are labeled A, B, C, D.

KANKELBORG et al. (see 466, 529)

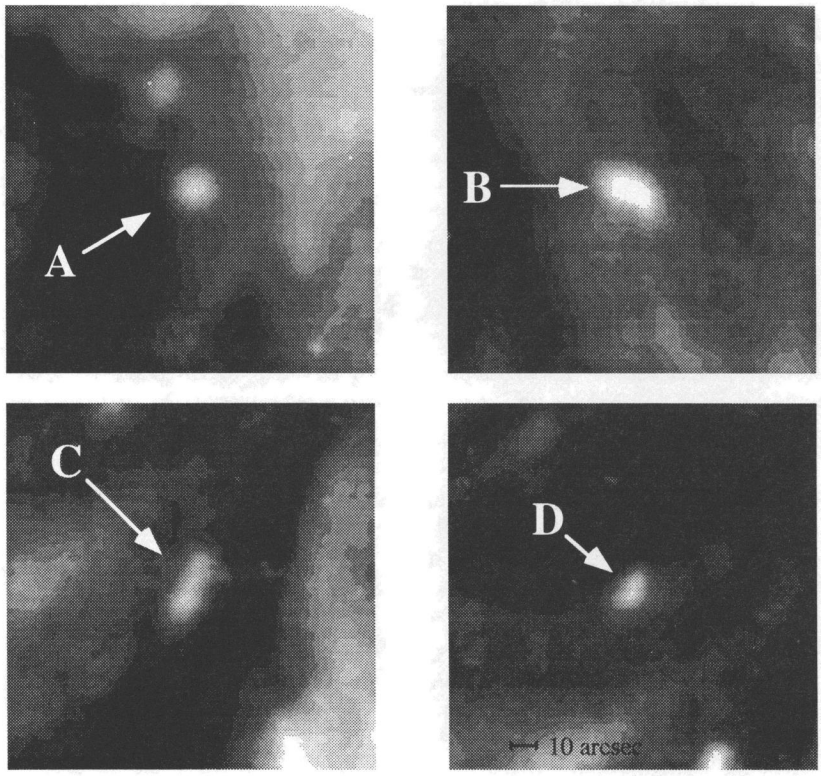

FIG. 3.—Detail of X-ray bright points in Fe XII (from a digitized image of the flight negative)

(especially D) appear to be misaligned with the loop axis in the Fe XII and Lyα images. This appearance is partly due to foreshortening. But even after stretching the images to compensate for foreshortening, we find differences in apparent orientation between the rocket data and the magnetogram. This probably indicates convection of the footpoints during the 4.5 hr period between the magnetogram and the MSSTA rocket flight.

There are at least 26 XBPs in the MSSTA images, most with similar apparent morphology, as well as a number of more diffuse fine-scale features that are sources of plumes and have unipolar magnetic fields. The latter have been

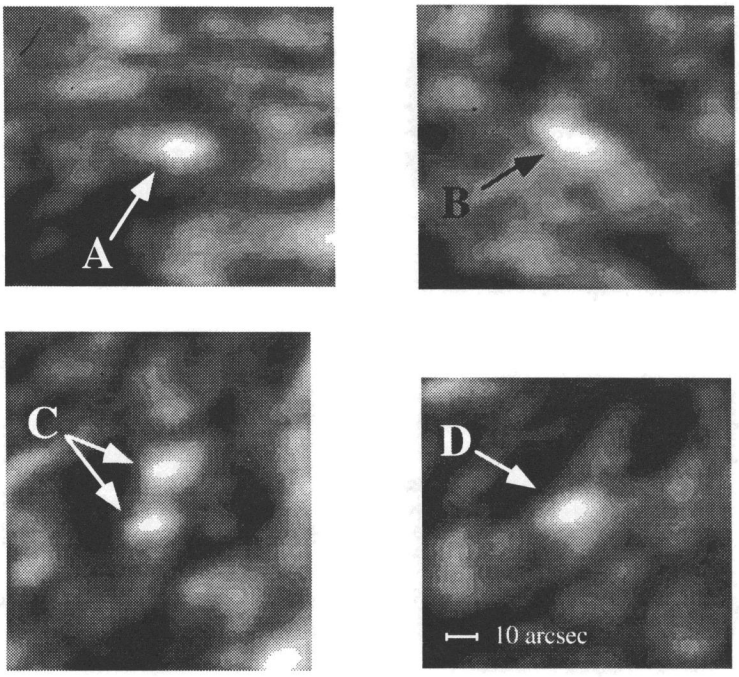

FIG. 4.—Detail of XBP footpoints in H Lyα (from a digitized image of the flight negative)

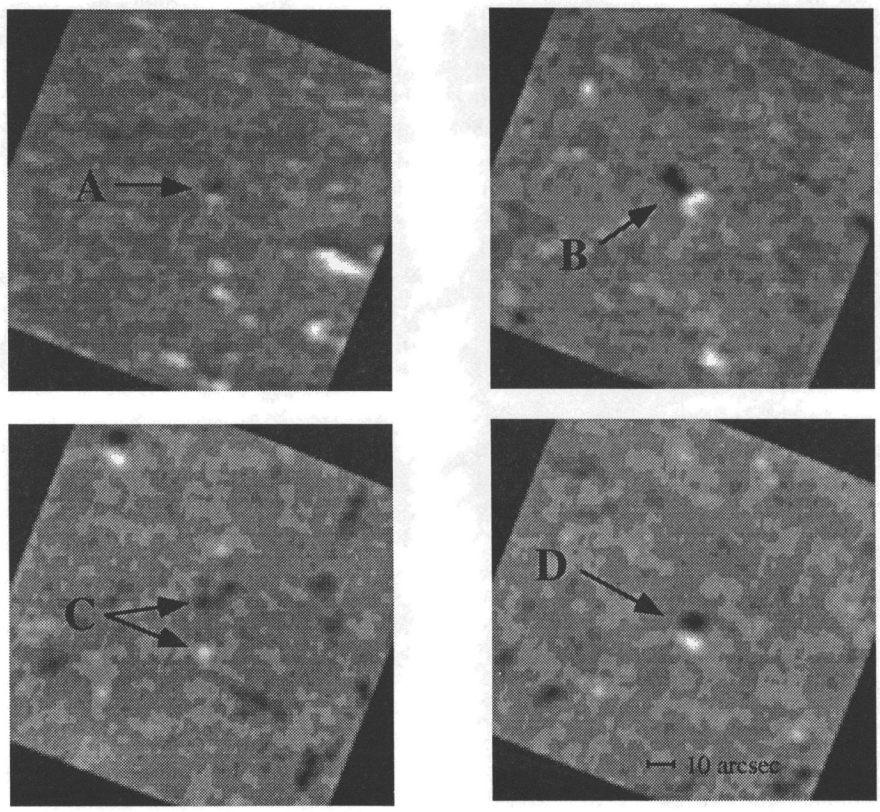

FIG. 5.—Line-of-sight magnetic field in the photosphere beneath each of the four XBPs (from a KPNO magnetogram taken 4.5 hr before the MSSTA rocket flight).

analyzed by Allen (1995; Allen et al. 1996). Although the magnetogram was taken 4.5 hr before the MSSTA rocket launch, at least 18 of the 26 XBPs indentified so far correspond to apparent magnetic dipoles in the KPNO magnetogram. Of the remaining eight, one corresponds to a quadrupole, one corresponds to a unipole, one appears to have two footpoints of the same polarity, and five have no evident magnetic signature. Of these five, four are close to the limb and might not appear on a line-of-sight magnetogram (they are 10″–170″ from the limb). Unfortunately, we do not have a magnetogram taken several hours after the launch for comparison, but the data we do have support the notion that bright points are associated with preexisting magnetic elements rather than with emerging flux (cf. Webb et al. 1993).

All but one of the 26 observed bright points correspond with unusually bright network elements in the Lyα image. In fact, virtually every coronal feature has extremely bright footpoints in Lyα. It is our hypothesis that these bright network elements are heated primarily by thermal conduction from the corona. Fontenla, Avrett, & Loeser (1990) have developed numerical models of the transition region heated by conduction from the corona. This idea is pursued further in §§ 4.2 and 5.3.

3. DATA REDUCTION

This section describes the procedures used for reducing bright point data from digitized flight negatives. The results of this data reduction are presented in Table 1.

Length measurements.—Bright-point images were first corrected for foreshortening. The half-length L (see Fig. 6) was estimated based on footpoint separation in the Lyα image, assuming semicircular geometry:

$$L = \tfrac{1}{4}\pi \times \text{footpoint separation} .$$

For bright points A and D, separate footpoints were not resolved. The footpoint separation was therefore estimated by measuring along the semimajor axis of the elliptical spot containing the footpoints.

Temperature estimation.—At the time this analysis was performed, adequate film calibrations were not available for most of the other EUV images obtained during the MSSTA

TABLE 1

BRIGHT POINT MEASUREMENTS

Bright Point	L (10^8 cm)	T (10^6 K)	H Lyα Film Flux (10^{-5} ergs s^{-1})	193 Å Film Flux (10^{-5} ergs s^{-1})
A	3.5 ± 2	1.55 ± 0.25	7.5 ± 50%	1.3 ± 50%
B	6.5 ± 2	1.55 ± 0.25	8.0 ± 50%	2.6 ± 50%
C	11.4 ± 1	1.55 ± 0.25	9.3 ± 50%	0.57 ± 50%
D	3.5 ± 1	1.55 ± 0.25	7.6 ± 50%	0.54 ± 50%

flight. The usual techniques of spectral hardness ratios were therefore not available for estimating the temperature of the X-ray loops. However, the four bright points selected for this preliminary study all appear very clearly both in the 193 Å (Fe XII) and 44 Å (Si XII) images. This constrains the range of possible temperatures for the four bright points to (0.8–2.5) × 10^6 K. In the model (see § 4.1), the temperature was limited to (1.3–1.8) × 10^6 K, which corresponds to the intersection of the FWHM of the temperature-response kernels of the two telescopes (see § 4.3). In future studies, we will have calibrations available for several more EUV telescopes. Temperature will be left as a free parameter, and the model will be optimized to fit multispectral data.

Background subtraction and photometry.—Each bright-point image was first converted via film calibration from abstract pixel values to actual intensity units. Since bright points are isolated, pointlike features, the background in a small, square subimage containing an XBP was modeled by holding the pixels at the edges constant and then point-relaxing the interior. The result was then subtracted from the original image. Finally, the background-subtracted bright point was integrated to find the energy per unit time, Φ, deposited on the film.

4. ANALYSIS

4.1. *Loop Model*

We use a simple one-dimensional, symmetric, quasi-static loop model similar to that of Vesecky, Antiochos, & Underwood (1979) to describe the X-ray loop from 10^5 K to its maximum temperature, which is assumed to occur at the loop's summit. The loop is further assumed to be of constant cross section since this seems to agree with most observations of actual loops, both our own and those of other investigators (see, e.g., Klimchuk et al. 1992). This assumption is revisited in § 5.3. Conservation of energy is expressed as

$$\frac{dF_C}{dx} = \epsilon - n^2\Lambda(T) , \tag{1}$$

where F_C is the conductive flux through a unit area and ϵ is the heating rate per unit volume. We use the Spitzer conductivity,

$$F_C = -10^6 T^{5/2} \frac{dT}{dx} . \tag{2}$$

Since conduction is extremely effective at coronal temperatures, the spatial dependence of the heating function is unimportant (see, e.g., Durrant & Brown 1989); we therefore use constant ϵ. The radiative loss function $\Lambda(T)$ is approximated by power laws,

$$\Lambda(T) = \Lambda_s (T/T_s)^M , \tag{3}$$

with parameters Λ_s, T_s, and M taken from Vesecky et al. (1979). We use a constant heating rate per unit volume, ϵ. Gravity is neglected in this model since the loops we are studying are very small compared to the gravitational scale height. Thus,

$$P = 2n_e k_B T = \text{const} . \tag{4}$$

Because of the above simplifying assumptions, it was possible to reduce the nonlinear second-order differential equation (1) to first order, separate variables, and write a definite-integral solution equivalent to that of Rosner, Tucker & Vaiana (1978). This made the integration of our numerical model fairly quick, so that iterative fitting of the model to measurements could be carried out on a personal computer. The integration of the model was tested first with a simple trapezoid rule and then finally implemented with a (much faster) fifth-order open Romberg routine (see Press et al. 1988). The model results are in rough agreement with the scaling law of Rosner et al. (1978),

$$T_{top}^2 = 10^{-6.1} n_{top} L . \tag{5}$$

However, we caution the reader that the scaling law is not a necessary consequence of our quasi-static loop model (see § 5.2).

4.2. *Transition Region*

Below ~10^5 K, ambipolar diffusion becomes an important consideration, and the type of model described in § 4.1 becomes inadequate. It is a common feature of most transition-region models (see, e.g., Fontenla et al. 1990) that virtually all of the energy conducted through the 10^5 K isotherm is emitted as H Lyα radiation. Therefore, we employ the Lyα flux as a measure of heat conducted to the chromosphere:

$$L_{Ly\alpha} = -2AF_{C0} , \tag{6}$$

where $L_{Ly\alpha}$ is the background-subtracted luminosity of both footpoints in Lyα, A is the cross-sectional area of the loop, and F_{C0} is the conductive flux at $T = 10^5$ K. This is represented diagrammatically in Figure 6.

4.3. *Instrument Response to the Solar Plasma*

The instrument response model relates the temperature and density of the plasma to the energy deposited on the detector (photographic film) of each telescope. Each of the MSSTA XUV telescopes is characterized by a temperature response kernel $K(T)$, which incorporates both telescope calibration and the emissivity due to collisional excitation of the optically thin coronal plasma (Deforest et al. 1991). The flux (in the sense of energy deposited per second) in the film plane of the telescope due to a coronal feature occupy-

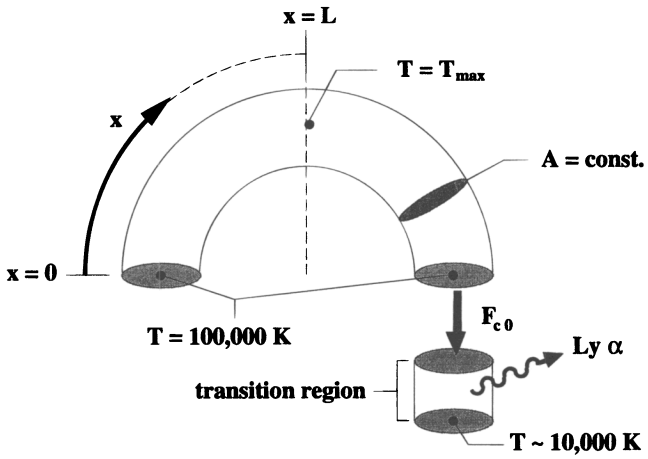

FIG. 6.—Sketch of the simple one-dimensional loop model used in this analysis.

ing a volume V is

$$\Phi = \frac{a^2}{2r^2} \int n_e^2 K(T)\, dV \,, \tag{7}$$

where a is the effective aperture of the telescope and $r = 1$ AU. The behavior of the loop model is such that most of the volume of the loop is at nearly constant temperature; the emission measure is strongly peaked at T_{max}. In this analysis, the volume integral in equation (7) has been approximated by taking the electron density and response kernel at T_{max} and multiplying by total volume of the loop. Comparison with the full calculation for one of the best-fit models (B) indicates that this procedure underestimates the flux by $\sim 25\%$, which is within the measurement errors estimated for the photographic film (see Table 1).

The film flux for the 1216 Å telescope is related to the H Lyα luminosity of a solar structure by the formula

$$\Phi_{Ly\alpha} = \frac{a^2}{2r^2} E_{Ly\alpha} L_{Ly\alpha} \,, \tag{8a}$$

where $E_{Ly\alpha}$ is the efficiency of the telescope ($\sim 0.34\%$). Combining equations (6) and (8a), one obtains

$$\Phi_{Ly\alpha} = \frac{-Aa^2}{r^2} E_{Ly\alpha} F_{C0} \,. \tag{8b}$$

4.4. *Computational Method*

For a particular choice of F_{C0}, n_{e0}, and ϵ, the loop model is integrated from the $T_0 = 10^5$ K isotherm up to the peak of the loop, where $dT/dx = 0$. The result is a determination of the half-length L, the maximum temperature T_{max}, and the temperature and density profiles of the loop (see Fig. 8). These results, along with a particular choice of A, can then be inserted into the instrument response model to solve for the resulting film fluxes for the telescopes. Thus the loop and instrument response models described in §§ 4.1 and 4.2 can be viewed as a mapping G from the variable space $\{A, \epsilon, F_{C0}, n_{e0}\}$ to the variable space $\{T_{max}, L, \Phi_{Ly\alpha}, \Phi_{Fe\ XII}\}$:

$$\begin{pmatrix} T_{max} \\ L \\ \Phi_{Ly\alpha} \\ \Phi_{Fe\ XII} \end{pmatrix} = G \begin{pmatrix} A \\ \epsilon \\ F_{C0} \\ n_{e0} \end{pmatrix} . \tag{9}$$

The variables in the column vector on the left-hand side of equation (9) are known, observed quantities, and the variables operated upon by G are unknowns. We wish to invert G and solve for the unknowns, taking into account the error ranges in the observed quantities. The approach we have taken is outlined in Figure 7. The process begins with a first guess for A, ϵ, F_{C0}, and n_{e0}. The model G is applied, and then the badness of fit of the model output to the observed

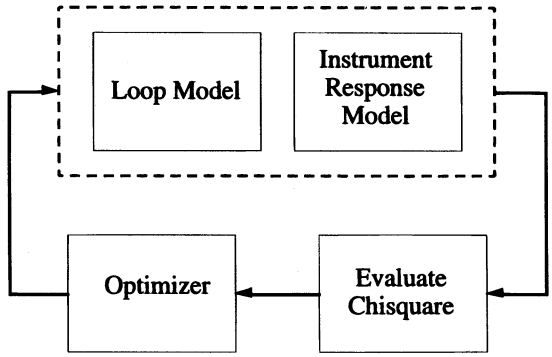

FIG. 7.—Block diagram of algorithm for fitting the XBP model to observational data.

quantities is evaluated based on a χ^2 statistic. An optimization routine attempts to minimize χ^2 by successive guesses of the input parameters. The downhill simplex method (Press et al. 1988) was chosen to perform this optimization because of its robustness and ease of implementation.

An attempt was made to discover any additional solutions that might fit the observational data. Regardless of what initial parameters were chosen, the model always converged to the same unique solution for each bright point. The solutions obtained appear to be uniquely determined.

Since the number of knowns equals the number of unknowns in equation (9), it should be feasible to exactly reproduce the observed data by an appropriate choice of the four unknowns. Unfortunately, it is not possible to test the model without more data. In a future paper, we intend to include measured fluxes from at least two more telescopes. Then it will be possible to relax or totally remove the overall temperature constraint in the fitting process, so that loop temperature will be determined more rigorously; because the model will be overconstrained, it may be possible, to some degree, to verify the assumptions of the model.

5. RESULTS AND DISCUSSION

5.1. *Model Results*

Table 2 shows the inferred electron densities and coronal heating rates for each of the four XBPs. For convenience, the heating rate per unit footpoint area (ϵL) has also been included. These values are of the same order as the rate of 1.5×10^7 ergs cm^{-2} s^{-1} measured by Neupert, Nakagawa, & Rust (1975) for a large ($\sim 10^{10}$ cm) active region struc-

TABLE 2

LOOP MODEL RESULTS

Bright Point	χ^2 ($\times 10^{-5}$)	ϵ (ergs cm^{-3} s^{-1})	ϵL (ergs cm^{-2} s^{-1})	F_{C0} (ergs cm^{-2} s^{-1})	n_{top} (cm^{-3})	A (cm^2)
A	1.2	2.9×10^{-2}	1.0×10^7	-4.5×10^6	7.4×10^9	6.3×10^{16}
B	0.2	9.1×10^{-3}	5.9×10^6	-1.6×10^6	4.5×10^9	1.8×10^{17}
C	0.7	2.4×10^{-3}	2.7×10^6	-1.9×10^6	1.6×10^9	1.8×10^{17}
D	0.6	2.6×10^{-2}	9.1×10^6	-6.0×10^6	5.5×10^9	4.7×10^{16}

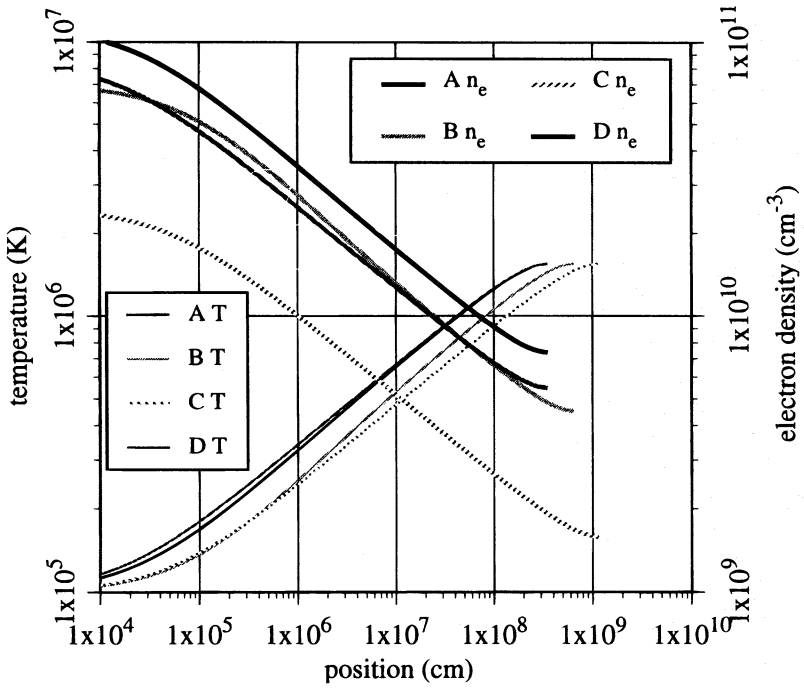

FIG. 8.—Temperature and density profiles based on model results for bright points A, B, C, and D

ture. Figure 8 shows the temperature and density profiles of the four loops, based on the results of the best-fit models.

5.2. *Agreement with the Scaling Law*

In Figure 9, the observed half-lengths of the XBPs are plotted against predicted lengths based on the scaling law (eq. [5]). Density values were taken from the model results in Table 2. The data from Rosner et al. (1978) are included for comparison. The scatter in the XBP data is not due to errors in measurement; the values of temperature, length, and density are known to be in perfect agreement with a static loop model. However, our model uses a different lower boundary condition than that of Rosner et al., who derived the scaling law using a loop model that extended down to 2×10^4 K, where the conductive flux is assumed to be negligible. This lower boundary condition is somewhat artificial in view of the finding of Fontenla et al. (1990), who showed that ambipolar diffusion enables the transition region to increase its radiative loss in H Lyα in response to high temperature gradients; the energy equation (eq. [1]) thus takes a different form below $\sim 10^5$ K. An equivalent (and more physically meaningful, from the point of view of our coronal model) assumption that may be used to derive the scaling law is that the radiative and conductive losses in the corona are approximately equal. This is only very roughly true, as evidenced by the lack of correlation between the EUV flux and the Lyα flux (Table 1). Nevertheless, the scatter in Figure 9 is no worse for the XBPs than for the data set used by Rosner et al., and the scaling law trend looks more convincing when viewed over a very wide range of length scales.

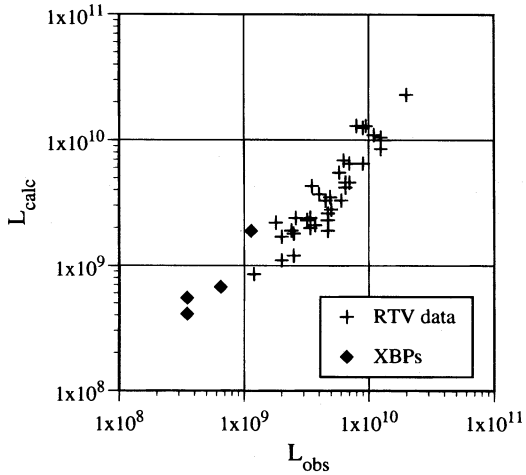

FIG. 9.—Comparison of observed half-length to that predicted by the scaling law. The XBP data extend the trend shown by Rosner et al. (1978).

5.3. *Magnetic Construction, Filling Factor, and Heating of the Transition Region*

The foregoing analysis has assumed constant cross-sectional area A. It is worth considering whether this is a tenable assumption and what the effect would be on the model if A were allowed to vary with temperature.

Certainly the X-ray–emitting portions of loops appear to have constant A. But there must be some constriction in area between the corona and the photosphere, where the field is concentrated into kilogauss bundles. Berger et al. (1995) have observed subarcsecond magnetic elements in the photosphere. Indirect evidence of highly constricted magnetic flux tubes at $\sim 10^5$ K comes from Dere et al. (1987) and Athay & Dere (1991), who derived plasma filling factors of order 10^{-3} in the lower transition region (LTR) based on data from the High Resolution Telescope and Spectrograph (HRTS) on Spacelab 2. Since it is commonly asserted that the filling factor in the corona is ~ 1 (but see Cargill 1994 for a review of the many inconsistent measurements), this naturally raises the question: do the XBP flux tubes change significantly in cross-sectional area between the LTR at 10^5 K and the corona at $\sim 10^6$ K? The preponderance of evidence seems to suggest that the struc-

tures responsible for most of the FUV emission in the LTR are thermally insulated from the coronal plasma (Dowdy, Rabin, & Moore 1986; Rabin & Moor 1984; Feldman 1983). Thus, what is called the lower transition region is probably not the thermal interface between the corona and the underlying solar atmosphere. Measurements of filling factors in C IV and other LTR lines in the quiet Sun therefore may not apply to the lower temperature portions of coronal structures. Feldman (1983) suggested that the "true" transition between corona and chromosphere corresponded to the lowest intensities observed in the FUV. Given the apparent correspondence between enhanced Lyα network elements and footpoints of bright coronal structures in the MSSTA data, we submit that the very brightest LTR features may also represent the "true" transition region. Similarly, images obtained during the MSSTA II flight of 1994 November (Walker et al. 1996), including a remarkable full-disk C IV image that resolves the discrete, spicule-like structures observed previously by HRTS, show a very striking correspondence between enhanced network in C IV, enhanced network in H Lyα, and the footpoints of structures in the low corona. If our hypothesis is correct, then the corona appears to supply substantial backheating, and the magnetic flux tubes leading downward from bright loops are therefore probably not very constricted at 10^5 K. Indirect evidence of moderate magnetic constriction in the "true" transition region is offered by Rabin (1991), who modeled coronal funnels in the quiet Sun. Rabin showed that the differential emission measure above $\sim 10^{5.3}$ K and several other observational constraints are best fitted by a bowl-shaped magnetic funnel with constriction factor $\Gamma = A(10^{6.2}\ \mathrm{K})/A(10^5\ \mathrm{K}) = 4$.

In order to explore the effect of magnetic constriction on our best-fit models, some models were calculated with a variable cross section $A(T) \propto T^{\alpha}$ (cf. Durrant & Brown 1989). This produces a strongly bowl-shaped funnel at the base of the loop, with $\Gamma = (T_{\max}/T_0)^{\alpha}$. Optimized best fits were found for $\Gamma = 4$, 16, and 240 for two of the bright points (A and B). The results for bright point B are represented in Figures 10 and 11. The model for bright point A behaved identically, and we would expect the same scaling to hold for all of the models. We therefore infer approximate scaling relations for the best-fit model parameters:

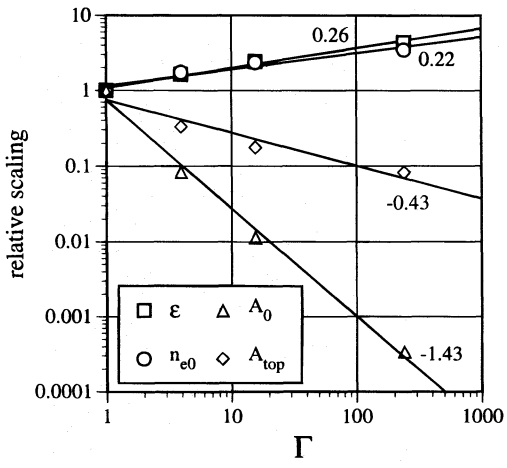

FIG. 10.—Scaling of best-fit model parameters for bright point B as a function of expansion factor, Γ. A best-fit power law is shown for each, with the power-law index displayed. Models for the other XBPs scale similarly.

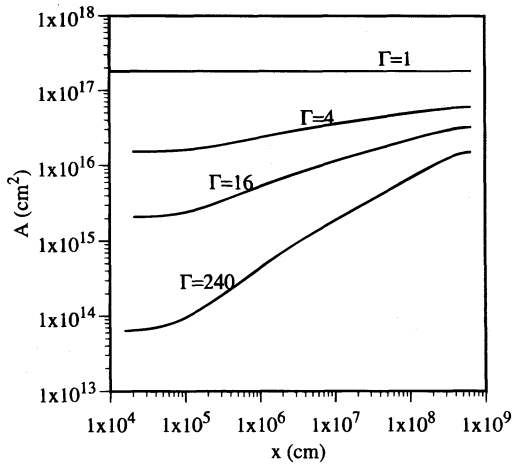

FIG. 11.—$A(x)$ of bright point B for various values of Γ

$$\epsilon \propto P \propto \Gamma^{1/4}\ , \tag{10a}$$

$$F_{C0} \propto A_0^{-1} \propto \Gamma^{3/2}\ , \tag{10b}$$

$$A_{\mathrm{top}} \propto \Gamma^{-1/2}\ . \tag{10c}$$

One of the surprising features of these results is that, in order to fit both the Lyα and Fe XII data, the models with constricted footpoints must be narrower overall. This in turn places a heavy burden on the conductive flux to supply enough energy to account for the observed emissions in Lyα. It should be emphasized that the above results were derived from a model assuming local thermodynamic equilibrium and classical heat transport, which must break down at sufficiently high tempeature gradients. Values of F_{C0} in excess of 10^8 ergs cm^{-2} s^{-1} certainly violate the assumptions inherent in this analysis.

5.4. *Are the Estimates for the Cross Section Geometrically Reasonable?*

Since the cross section A is estimated by the model rather than by direct measurements, it is best to check whether the inferred value of A is reasonable. The image data are at least capable of putting an upper limit on A . In order to make these considerations as general as possible, the effects of filling factor and magnetic constriction are included.

Let ϕ be the filling factor at 10^5 K, and let A denote the cross section for $\Gamma = 1$ (Table 2). The area occupied by the footpoint in the LTR is then $A_0\phi^{-1} \sim A\Gamma^{-3/2}\phi^{-1}$ (eq. [10]). The footpoint cannot be much larger than the size observed in Lyα, so we insist that $A\Gamma^{-3/2}\phi^{-1} \lesssim L^2$. Solving for the filling factor,

$$\phi \gtrsim \phi_{\min} \equiv A\Gamma^{-3/2}L^{-2}\ . \tag{11}$$

The estimated area is reasonable for any filling factor greater than $\phi_{\min}$. From the point of view of constructing a best-fit model, if $\phi_{\min} \gg 1$, then it is impossible to satisfy this relation, and there is too much radiation in Lyα to be accounted for by classical conduction from the corona. The values of $\phi_{\min}$ derived from the constant cross section models for bright points A, B, C, and D are 0.51, 0.43, 0.14, and 0.38, respectively. Since the footpoints of bright point C in Figure 4 appear much smaller than L, $\phi_{\min}$ may be revised upward to ~ 0.7. All of these estimates for $\phi_{\min}$ are less than 1, but not much less. It will be interesting to see

whether all the bright points observed by MSSTA satisfy this test.

If we assume that the filling factor in the corona is 1, then the cross section in the corona is $A_{top} \sim A\Gamma^{-1/2}$ (eq. [10]). If the loops are approximately circular in cross section, then A_{top} cannot be much larger than the square of the width observed in soft X-rays:

$$A\Gamma^{-1/2} \lesssim d^2_{\text{Fe XII}} . \quad (12)$$

For bright points A, B, and D, $d_{\text{Fe XII}} \sim L$; the X-ray loop of bright point C has an apparent width of $\sim 4 \times 10^8$ cm. Equation (12) is satisfied by all four bright points for all $\Gamma \geq 1$, and so the best-fit values of A are deemed reasonable for the coronal portions of the loops.

6. CONCLUSIONS

Our observations are in agreement with other investigations that have found that compact XBPs are bipolar, closed magnetic structures. All of the XBPs have strong chromospheric signatures in H Lyα. Moreover, the results obtained from modeling indicate that, as long as the footpoints of the loops are not greatly constricted, classical conduction from the corona can pump enough energy downward through the 10^5 K isotherm to account for all of the observed flux from the Lyα network elements that mark the XBP footpoints. We have argued that the energy distribution mechanisms at work in the lower transition region (e.g., ambipolar diffusion, as discussed by Fontenla et al. 1990) will allow most of that energy to be radiated away in Lyα. This echoes the findings of Habbal & Withbroe (1981), who also observed that temporal variations in the coronal brightness of XBPs tend to precede variations in the transition region and chromosphere.

The results of the static loop model are in rough agreement with the scaling law given by Rosner et al. (1978). Deviations from ths scaling law are attributed to the inequality of radiative and conductive losses in the bright points, as evidenced by the lack of proportionality between Fe XII and H Lyα flux measurements.

We extend our gratitude to Karen Harvey of Solar Physics Research Corporation for providing rotated KPNO magnetograms and for helpful discussions about bright points. We are indebted to Piero Pianetta, Michael Rowen, and others at SSRL for providing us with an excellent facility for calibrations. We thank Craig Deforest, Maxwell Allen, and the whole MSSTA team for their patience with endless film calibrations, and for many enjoyable conversations on solar physics. Finally, we thank the Lockheed SPARCS sounding rocket team and the personnel at White Sands Missile Range and at NASA Wallops Island Flight Facility, who have made solar rocketeering an enjoyable and scientifically rewarding experience. This work was partially supported by NASA grant NSG-5131.

REFERENCES

Allen, M. J. 1995, Ph.D. thesis, Stanford Univ.
Allen, M. J., Walker, A. B. C., Jr., Hoover, R. B., & Barbee, T. W. 1996, Sol. Phys., submitted
Athay, R. G., & Dere, K. P. 1991, ApJ, 379, 776
Berger, T., Schrijver, C. J., Shine, R. A., Tarbell, T. D., Title, A. M., & Scharmer, G. 1995, ApJ, 454, 531
Cargill, P. J. 1994, ApJ, 422, 381
Deforest, C. E., et al. 1991, Opt. Eng., 30, 1125
Dere, K. P., Bartoe, J.-D. F., Brueckner, G. E., Cook, J. W., & Socker, D. G. 1987, Sol. Phys., 114, 223
Dowdy, J. F., Rabin, D., & Moore, R. L. 1986, Sol. Phys., 105, 35
Durrant, C. J., & Brown, S. F. 1989, Proc. Astron. Soc. Australia, 8, 137
Feldman, U. 1983, ApJ, 275, 367
Fontenla, J. M., Avrett, E. H., & Loeser, R. 1990, ApJ, 355, 700
Golub, L. 1980, Phil. Trans. Roy. Soc. London A, 297, 595
Golub, L., Nystrom, G., Herant, M., Kalata, K., & Lovas, I. 1990, Nature, 344, 842
Habbal, S. R., Dowdy, J. F., & Withbroe, G. L. 1990, ApJ, 352, 333
Habbal, S. R., & Withbroe, G. L. 1981, Sol. Phys., 69, 77
Hoover, R. B., Walker, A. B. C., Jr., Deforest, C. E., Allen, M. J., & Lindblom, J. F. 1991, Opt. Eng., 30, 1116
Klimchuk, J. A., Lemen, J. R., Feldman, U., Tsuneta, S., & Yutaka, U. 1992, PASJ, 44, L181
Moses, D., et al. 1994, ApJ, 430, 913
Neupert, W. M., Nakagawa, Y., & Rust, D. M. 1975, Sol. Phys., 43, 359
Press, W. H., Flannery, B. P., Teukolsky, S. A., & Vetterling, W. T. 1988, Numerical Recipes in C (Cambridge: Cambridge Univ. Press)
Rabin, D. 1991, ApJ, 383, 407
Rabin, D., & Moore, R. 1984, ApJ, 285, 359
Rosner, R., Tucker, W. H., & Vaiana, G. S. 1978, ApJ, 220, 643
Strong, K. T., Harvey, K., Hirayama, T., Nitta, N., Shimizu, T., & Tsuneta, S. 1992, PASJ, 44, L161
Vesecky, J. F., Antiochos, S. K., & Underwood, J. H. 1979, ApJ, 233, 987
Walker, A. B. C., Jr., Barbee, T. W., Jr., Hoover, R. B., Kankelborg, C. C., Deforest, C. E., Martínez-Galarce, D. S., & Plummer, J. E. 1996, in preparation
Walker, A. B. C., Jr., Barbee, T. W., Jr., Lindblom, J. F., & Hoover, R. B. 1988, Science, 241, 1781
Walker, A. B. C., Jr., Hoover, R. B., & Barbee, T. W., Jr. 1993 in Physics of Solar and Stellar Coronae, ed. J. Linsky & S. Seir (Dordrecht: Kluwer), 83
Walker, A. B. C., Jr., Lindblom, J. F., O'Neal, R. H., Alen, M. J., Barbee, T. W., Jr., & Hoover, R. B. 1990, Opt. Eng., 29, 582
Webb, D. F., Martin, S. F., Moses, D., & Harvey, J. W. 1993, Sol. Phys., 144, 15